

high frequency in high-risk pancreatic cancers (13). The M50R Fan1 variant, which cosegregates with pancreatic cancer in two separate families, is a strong candidate pancreatic cancer predisposition gene. M50 lies in the UBZ domain of Fan1 (Fig. 4C). Similar to the UBZ* mutation (C44A+C47A), the Fan1 M50R mutation abolished Fan1 foci but rescued the MMC sensitivity of U2OS Fan1^{-/-} cells (Fig. 4, D and E). The M50R mutant failed, however, to prevent chromosome abnormalities induced by HU or MMC in Fan1^{-/-} cells (Fig. 4F). Moreover, expression of wild-type Fan1 in Fan1^{-/-} cells restored normal track length in HU, but the Fan1 M50R mutant failed to do so (Fig. 4G). Therefore, the Fan1 M50R variant associated with high-risk pancreatic cancers causes unrestrained replication fork progression and chromosomal instability known to drive carcinogenesis.

In this study, we made the unexpected finding that although Ub-Fancd2 recruits Fan1 to ICL-blocked replication forks, this is not required for ICL repair judged by MMC sensitivity and G₂ arrest. Instead, Fan1 recruitment is vital for protective responses when forks stall, even in the absence of DNA cross-links. Cells defective in Fan1 recruitment, or activity, show a high frequency of chromosome abnormalities and increased fork rate when forks are forced to stall. The mechanisms underlying these defects are not yet clear, but cells depleted of the HLTf translocase or RAD51 recombinase, which both drive fork reversal, show longer replication tracks in HU, similar to Fan1-defective cells (14, 15). Therefore, Fan1 recruitment and activity might promote fork reversal, but this remains to be tested. It is not yet clear whether the chromosome abnormalities seen after fork stalling in Fan1-defective cells are related to the increased fork speed or whether they arise independently. It seems counter-intuitive, perhaps, that a nuclease activity is required to prevent chromosome breaks at stalled forks. One potential explanation is that Fan1 cleaves stalled forks in a way that enables replication to resume after fork stalling, consistent with a recent report that Fan1 promotes replication fork recovery (16). Failure of Fan1-mediated fork processing may result in the persistence of structures that are cleaved inappropriately by other nucleases, leading to forks breaking in a way that is refractory to repair.

Our observations that Fan1 nuclease activity and interaction with Ub-Fancd2 prevent cancers prompt future investigations as to whether cancer predisposition associated with FA might be caused by defective fork processing, as opposed to defective ICL repair. Identifying a separation-of-function Fan1 mutant affecting ICL repair but not stalled fork processing would be valuable for these efforts. Besides pancreatic cancer, germline mutations in Fan1 have been identified in colon cancer (17). Loss of heterozygosity (LOH) has not been observed in tumors from the M50R carriers or in Fan1-mutated colon cancers (13, 17). Epigenetic inactivation of Fan1, haplo-insufficiency, or dominant-negative effects may provide explana-

tions, but these ideas remain to be investigated. KIN caused by biallelic Fan1 mutations is a very rare disease, but early-onset cancers were reported in two affected families (17). These reports, together with the present study, are consistent with Fan1 acting as a tumor suppressor with multiple roles in genome maintenance vital for preventing human diseases.

REFERENCES AND NOTES

1. A. D. Auerbach, *Mutat. Res.* **668**, 4–10 (2009).
2. H. Kim, A. D. D'Andrea, *Genes Dev.* **26**, 1393–1408 (2012).
3. I. Garcia-Higuera *et al.*, *Mol. Cell* **7**, 249–262 (2001).
4. C. MacKay *et al.*, *Cell* **142**, 65–76 (2010).
5. K. Kratz *et al.*, *Cell* **142**, 77–88 (2010).
6. T. Liu, G. Ghosal, J. Yuan, J. Chen, J. Huang, *Science* **329**, 693–696 (2010).
7. A. Smogorzewska *et al.*, *Mol. Cell* **39**, 36–47 (2010).
8. W. Zhou *et al.*, *Nat. Genet.* **44**, 910–915 (2012).
9. I. M. Munoz, P. Szyniarowski, R. Toth, J. Rouse, C. Lachaud, *PLOS ONE* **9**, e109752 (2014).
10. K. Schlacher, H. Wu, M. Jasin, *Cancer Cell* **22**, 106–116 (2012).
11. G. Lossaint *et al.*, *Mol. Cell* **51**, 678–690 (2013).
12. S. Houghtaling *et al.*, *Genes Dev.* **17**, 2021–2035 (2003).
13. A. L. Smith *et al.*, *Cancer Lett.* **370**, 302–312 (2016).
14. R. Zellweger *et al.*, *J. Cell Biol.* **208**, 563–579 (2015).
15. A. C. Kile *et al.*, *Mol. Cell* **58**, 1090–1100 (2015).
16. I. Chaudhury, D. R. Stroik, A. Sobek, *Mol. Cell Biol.* **34**, 3939–3954 (2014).
17. N. Seguí *et al.*, *Gastroenterology* **149**, 563–566 (2015).

ACKNOWLEDGMENTS

We are grateful to J. Hastie, H. MacLauchlan, and the Antibody Production Team at Division of Signal Transduction Therapy (DSTT) and the DNA Sequencing Service at the School of Life Sciences, University of Dundee. We thank Centre for Interdisciplinary Research Resource Unit (CIRRU) staff, especially L. Malone and C. Clacher, for help with animal husbandry and G. Gilmour and E. Forsyth for help with genotyping. We thank L. Oxford and L. Stevenson (Veterinary Diagnostic Services, University of Glasgow) for support with tissue processing. We thank A. d'Andrea for Fancd2^{-/-} mice. We are grateful to L. Feeney for critical reading of this manuscript. We thank A. Connor, A. Smith, S. Gallinger, and G. Zogopoulos for communicating data prior to publication. C.L. is the recipient of a Marie Curie Intra-European fellowship. A.M. was supported by Wellcome Trust Investigator Award WT096598MA to J.J.B. This study was supported by the Medical Research Council (MRC) and the pharmaceutical companies supporting the DSTT (AstraZeneca, Boehringer-Ingelheim, GlaxoSmithKline, Merck KgaA, Janssen Pharmaceutica, and Pfizer) associated with the MRC Protein Phosphorylation and Ubiquitylation Unit. Fan1 nuclease-defective mice are available from J.R. under a material transfer agreement with the University of Dundee.

SUPPLEMENTARY MATERIALS

www.sciencemag.org/content/351/6275/846/suppl/DC1
Materials and Methods
Figs. S1 to S6
References

1 October 2015; accepted 11 January 2016
Published online 21 January 2016
10.1126/science.aad5634

NEUROSCIENCE

Neurons diversify astrocytes in the adult brain through sonic hedgehog signaling

W. Todd Farmer,¹ Therése Abrahamsson,¹ Sabrina Chierzi,¹ Christopher Lui,¹ Cristian Zaelzer,¹ Emma V. Jones,¹ Blandine Ponroy Bally,¹ Gary G. Chen,^{2,3} Jean-Francois Thérout,^{2,3} Jimmy Peng,^{4,5} Charles W. Bourque,¹ Frédéric Charron,^{4,5} Carl Ernst,^{2,3,6,7} P. Jesper Sjöström,¹ Keith K. Murai^{1*}

Astrocytes are specialized and heterogeneous cells that contribute to central nervous system function and homeostasis. However, the mechanisms that create and maintain differences among astrocytes and allow them to fulfill particular physiological roles remain poorly defined. We reveal that neurons actively determine the features of astrocytes in the healthy adult brain and define a role for neuron-derived sonic hedgehog (Shh) in regulating the molecular and functional profile of astrocytes. Thus, the molecular and physiological program of astrocytes is not hardwired during development but, rather, depends on cues from neurons that drive and sustain their specialized properties.

Astrocytes have fundamental roles in nearly all aspects of brain function, including extracellular ion and neurotransmitter homeostasis, neurometabolism, and cerebrovasculature control (1–3). Prime examples are pH-sensing brainstem astrocytes that mediate respiratory control (4) and AMPA (α-amino-3-hydroxy-5-methyl-4-isoxazolepropionic acid)-type glutamate receptor-expressing glia that function in cerebellar motor learning (5). Distinct patterns of transcription (6, 7) implicate select

genetic programs and possibly distinct signaling mechanisms that establish astrocyte subtypes (2, 8). These processes participate in early developmental patterning events to promote astrocyte heterogeneity in vivo (9–12).

We explored how molecular features of astrocytes are created and sustained in the mature mouse brain. Because of the complexity of astrocyte heterogeneity in brain areas such as the cerebral cortex, we focused on the cerebellar cortex, which contains two specialized astrocyte

types, Bergmann glial cells (BGs) and velate astrocytes (VAs), that have distinct cell positioning, morphology, and molecular composition (13, 14). BGs localized within the Purkinje cell (PC) layer extend processes that enwrap PC dendrites and

¹Centre for Research in Neuroscience, Department of Neurology and Neurosurgery, Brain Repair and Integrative Neuroscience Program, The Research Institute of the McGill University Health Centre, Montreal General Hospital, Montreal, Quebec, Canada. ²Department of Psychiatry, McGill University, Montreal, Quebec, Canada. ³McGill Group for Suicide Studies, Douglas Hospital, Montreal, Quebec, Canada. ⁴Molecular Biology of Neural Development, Institut de Recherches Cliniques de Montréal, Department of Medicine, University of Montreal, Montreal, Quebec, Canada. ⁵Department of Biology, McGill University, Montreal, Quebec, Canada. ⁶Department of Human Genetics, McGill University, Montreal, Quebec, Canada. ⁷Douglas Hospital Research Institute, Verdun, Quebec, Canada.

*Corresponding author. E-mail: keith.murai@mcgill.ca

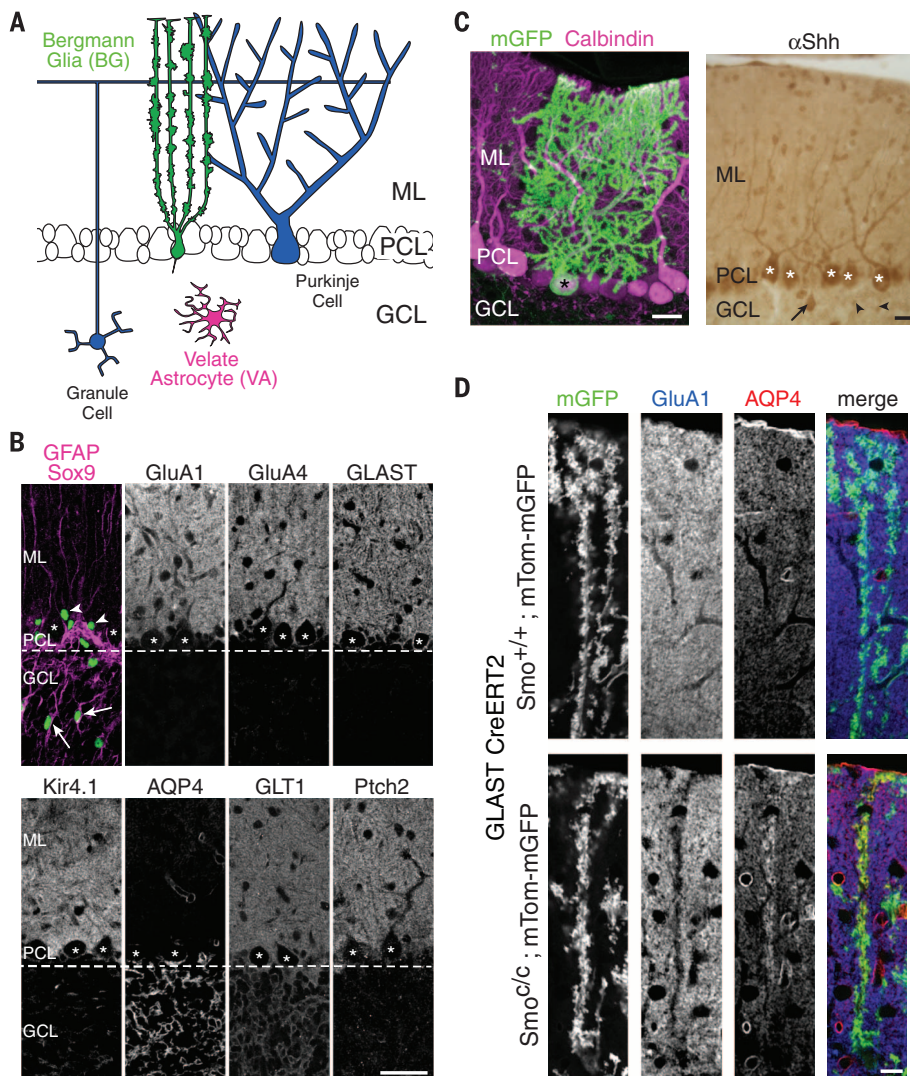


Fig. 1. Astrocytes in cerebellar cortex, expression of Shh, and Smo deletion. (A) BG (green) with soma in the Purkinje cell layer (PCL) and processes in the molecular layer (ML), and VAs (magenta) in GCL. (B) Immunofluorescence microscopy for proteins in BGs and VAs. (C) Expression of Shh in PCs expressing calbindin (magenta, asterisks), GCs (right, arrowheads), and interneurons (right, arrow) in Shh reporter mice and after Shh immunolabeling. (D) Removal of Smo through Cre recombination at 5 weeks and analysis 4 weeks later ($n = 6$ pairs). Scale bars: (B) 30 μm . (C) 15 μm . (D) 10 μm .

synapses (Fig. 1A). In contrast, VAs in the granule cell layer (GCL) surround granule cells (GCs) and mossy fiber glomeruli (Fig. 1A) (15). BGs and VAs display distinct, but overlapping, molecular profiles. Although BGs and VAs show comparable expression of genes, including *GFAP* (glial fibrillary acidic protein), *Sox9* [*SRY*-related high mobility group (HMG)-box gene 9], and *GLT1* (glutamate transporter 1), BGs are enriched in AMPA receptors GluA1 and GluA4, and GLAST (glial high-affinity glutamate transporter) (Fig. 1B) (5). VAs, in contrast, have low amounts of GluA1, GluA4, and GLAST and large amounts of the water channel aquaporin 4 (AQP4) (Fig. 1B) (16). Note that components of the sonic hedgehog (Shh) signaling pathway, a developmental morphogen pathway (17, 18), including the *Gli* transcription factor and Shh receptors Patched

(patched domain-containing protein) 1 and 2 (Ptch1/2), are also enriched in mature BGs but not VAs (www.brain-map.org; www.gensat.org) (Fig. 1B). Ptch2 and Smoothed (Smo) are also expressed by cultured cerebellar astrocytes expressing GLAST (fig. S1).

In the developing central nervous system (CNS), various cells produce Shh to regulate cell specification, axon guidance, and cell proliferation (17, 18). To identify which cells produce Shh in the mature brain, we used a mouse line that produces tamoxifen-sensitive Cre recombinase from the Shh gene locus (fig. S2A). Cre activation with tamoxifen in >5-week-old mice revealed that PCs, GCs, and interneurons expressed Shh (Fig. 1C and fig. S2, B to E). Immunolabeling for Shh showed localization in neurons, including PCs, and an overall enrichment in the molecular layer (Fig. 1C and fig. S2, F and G). To determine whether Shh signaling regulates mature BGs in vivo, we removed the Shh signal transducer Smo from BGs using controlled activation of Cre with tamoxifen in astrocytes expressing GLAST (GLAST CreERT2) (fig. S3A) (19, 20). Quantitative reverse transcriptase polymerase chain reaction (qRT-PCR) showed a 24% loss of *Smo* mRNA after Cre activation (fig. S3B), an amount that did not disrupt cerebellar organization or motor performance (fig. S3C). BGs lacking Smo extended processes that enwrapped PC dendrites, detected by staining of calbindin, and spines, seen by staining of metabotropic glutamate receptor 1 (mGluR1) (fig. S4).

Although Smo was not essential for the structure of BGs, Smo regulated expression of molecules that confer BG specialized properties (5). Shh signaling sustained GluA1 expression and prevented expression of AQP4 (Fig. 1D and fig. S3D). Virally expressed Cre in patches of BGs (Fig. 2A) revealed that Smo was needed for expression of GluA1, GluA4, GLAST, the inward rectifying potassium channel Kir4.1 (21), and Ptch2 (Fig. 2, B and C, and fig. S5) (22). This loss was accompanied by an increase in the amount of AQP4 (Fig. 2, B and C). No changes were observed for GLT1 or overall anatomy (figs. S5 and S6). To assess physiological changes to BGs, we used AMPA uncaging to elicit AMPA-receptor responses in BGs (Fig. 2D). This showed reduced AMPA receptor-mediated currents after Smo loss (Fig. 2E). To determine whether Shh expressed by PCs maintains BG gene expression, we removed Shh from PCs using Cre (fig. S7A). BGs next to PCs lacking Shh had decreased amounts of GluA1, Kir4.1, and GLAST and increased amounts of AQP4 (Fig. 2F and fig. S7B), with no disruption to the presence or position of cells containing SOX9 or the expression of GLT1 (fig. S8).

Cerebellar VAs are exposed to lower amounts of Shh than BGs, as indicated by Shh immunolabeling (Fig. 1C) and the low amounts of Shh receptor Ptch2, which is positively regulated by Shh signaling (Fig. 1B). To test whether the Shh pathway could control VAs, constitutively active Smo (SmoM2) was expressed in VAs under the control of Cre (fig. S9A) (23). Virally and genetically induced expression of SmoM2 in VAs

reduced amounts of AQP4 and increased GluA1, GLAST, and Kir4.1 (Fig. 3, A to C, and fig. S9, B to D) without affecting cell proliferation (fig. S10). To determine whether increasing the Shh pathway allowed VAs to obtain an mRNA profile resembling that of BGs, we performed RNA sequencing (RNA-seq) on small groups of VAs and BGs individually isolated from fresh brain slices (Fig. 3D and fig. S11). This identified 415 mRNAs that significantly distinguish control VAs from BGs. Hierarchical clustering analysis based on these mRNAs showed that *SmoM2*-expressing VAs (*SmoM2* VAs) showed greater similarity to BGs than control VAs. Genes strongly expressed in control VAs like *Edn1* (*endothelin 1*) and *Tlr2* (*Toll-like receptor 2*) are substantially reduced in *SmoM2* VAs, whereas genes expressed in BGs like *Anxa7* (*annexin A7*) are up-regulated in *SmoM2* VAs (Fig. 3, E and F). Thus, Shh signaling drives specific changes in VAs, which causes them to acquire a molecular profile that is intermediate between a BG and a VA.

We also tested if Shh signaling regulates BGs during development by altering Shh signal-

ing at postnatal day 2 (P2) and analyzing mice at P15 (fig. S12). *Smo* deletion decreased amounts of GluA1 and increased amounts of AQP4 in developing BGs (fig. S13, A and B), whereas *SmoM2* expression increased abundance of GluA1, GluA4, and Kir4.1 in VAs (fig. S13, C and D). *SmoM2* expression led to a small, significant increase in proliferating glia that contained Ki67, which suggested that Shh signaling promotes cell division during early stages (fig. S14). Thus, cerebellar astrocytes use the Shh pathway at developing and adult stages to establish and sustain their molecular features.

Shh is expressed by neurons in several adult brain regions (24–26). To determine whether astrocytes in these areas respond to the Shh pathway, we expressed *SmoM2* in mature astrocytes (fig. S15) and examined the expression of proteins, including Kir4.1, which shows heterogeneous expression (Fig. 4 and fig. S15). In the hippocampus, *SmoM2* expression increased Kir4.1 protein in CA1 and dentate gyrus astrocytes and overall *Kir4.1* mRNA (Fig. 4, A to C, and figs. S15 and S16). *Kir4.1* mRNA was also decreased in Shh haploinsufficient mice, which showed re-

duced *Shh* and *Gli1* mRNA (Fig. 4D). Kir4.1 up-regulation also increased barium-sensitive Kir4.1 currents, as revealed by changes in the rectification index (Fig. 4, E to H, and fig. S17) (27). Similarly, Kir4.1 mRNA levels were reduced in cultured hippocampal astrocytes exposed to Shh pathway inhibitors (fig. S18) (27, 28). GLAST, GluA1, and GluA4 expression were unaffected (figs. S19 to S21). In cortical astrocytes, removal of *Smo* reduced Kir4.1 protein (fig. S22, A and B), whereas expression of *SmoM2* increased astrocyte Kir4.1 protein (fig. S22, C and D, and fig. S23). This was consistent with decreased and increased Kir4.1 mRNA in the cortex of Shh haploinsufficient and *SmoM2* mice, respectively (fig. S22, E and F). GLAST and AQP4 mRNAs remained unchanged in *SmoM2* and Shh haploinsufficient mice (figs. S22, S24, and S25).

We found that astrocytes depend on cues from mature neurons to control their complex molecular profile in vivo. This challenges the concept that astrocytes contain hardwired molecular and physiological programs that are fully determined during development and indicates that neurons

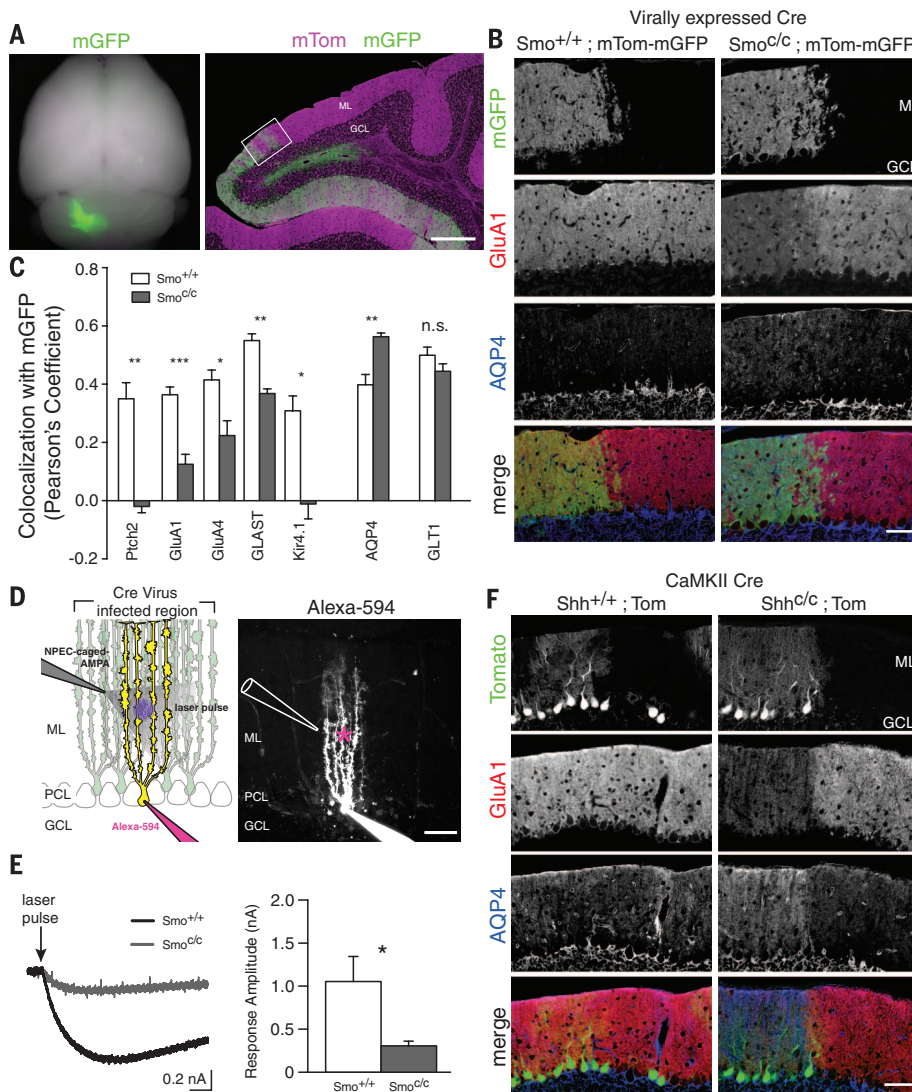
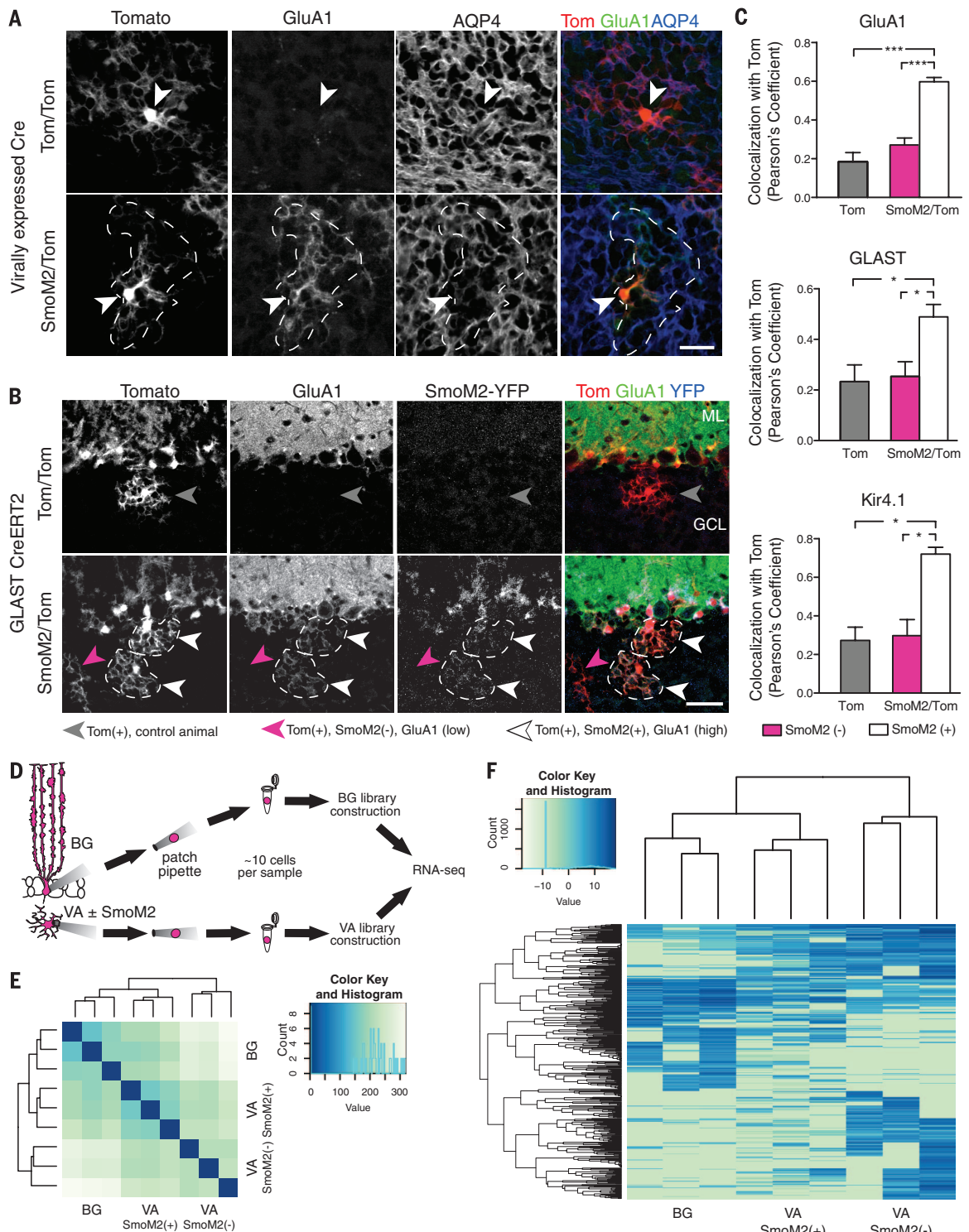


Fig. 2. Purkinje cells diversify BGs in the mature cerebellum.

(A) (Left) Fluorescence microscopy of membrane-targeted green fluorescent protein (GFP) (mGFP, green) in the cerebellum after viral expression of Cre. (Right) BGs that express mGFP or not (mTom; magenta). (B and C) *Smo* loss in BGs (green; virus delivered at >5 weeks, analyzed 4 weeks later) [Ptch2 ($n = 3$ pairs), GluA1 ($n = 5$), GluA4 ($n = 3$), GLAST ($n = 3$), Kir4.1 ($n = 3$), and AQP4 ($n = 5$)]. Protein expression determined by colocalization with mGFP reference protein. (D) (Left) Setup to elicit AMPA receptor currents in BGs. (Right) Patched BGs showing the location of the compound (*N*)-1-(2-nitrophenyl)ethylcarboxy-(*S*)- α -1-(2-nitrophenyl)ethylcarboxyamino-3-hydroxy-5-methyl-4-isoxazolepropionic acid (NPEC-AMPA) puff pipette and laser pulse (asterisk). (E) AMPA receptor currents in BGs. (Left) Representative trace and quantification of uncaging-evoked AMPA receptor currents in cells with *Smo* ($n = 7$; *Smo*^{+/+}) or not ($n = 8$; *Smo*^{C/C}). (F) Immunofluorescence detection of GluA1 and AQP4 in BG after loss of Shh from PCs ($n = 4$ pairs). Error bars represent SEM. Student's *t* test. * $P \leq 0.05$, ** $P \leq 0.01$, *** $P \leq 0.001$. Scale bars: (A) 300 μ m, (B), (D), and (F) 40 μ m.

Fig. 3. VAs acquire BG-like profiles upon Shh signaling.

(A) Immunofluorescence detection of GluA1 and AQP4 in VAs upon SmoM2 and Tomato expression after viral Cre expression (>5-week-old mice) (n = 4 pairs). (B) Detection of GluA1 in VAs expressing SmoM2 (white arrowheads) or not (gray and magenta arrowheads). (C) Quantification of GluA1, GLAST, and Kir4.1 in VAs through fluorescence colocalization with Tomato reference protein (n = 4). One-way analysis of variance (ANOVA) with Tukey's. (D) Experimental steps for single-cell RNA-seq. (E) Dendrogram representing a hierarchical clustering of gene expression distances between samples used in the single-cell RNA-seq experiment. Histogram shows a pseudo-color representation of the Euclidean distance matrix (from dark blue for zero distance to white for large distance). (F) Gene expression heat map from 415 differentially expressed genes identified in BGs compared with VAs. Colors reflect relative differences of each gene (y axis) for each sample (x axis). Unsupervised clustering trees are shown, and histogram shows relative expression level (white for lower expression and blue for higher expression). Error bars represent SEM. *P ≤ 0.05, ***P ≤ 0.001. Scale bars: (A) 20 μm, (B) 30 μm.



communicate with astrocytes to actively regulate their local environment in the brain. Neurons use Shh to control the properties of astrocytes and thus extend its role beyond cell proliferation, specification, and axon guidance during CNS development (17, 18). Surprisingly, astrocytes across

brain regions use Shh signaling differently. Cerebellar BGs use Shh signaling to promote glutamate detection (GluA1 and 4) and recovery (GLAST), as well as potassium homeostasis (Kir4.1) (27). This is presumably related to the dense glutamatergic inputs onto PCs in the molecular layer.

Note that cerebellar VAs acquire features of the BG transcriptome upon Shh signaling. Cortical and hippocampal astrocytes, in contrast, use Shh signaling for more selective regulation of Kir4.1. It is possible that neurons release an array of factors, including Shh, to create astrocyte complexity

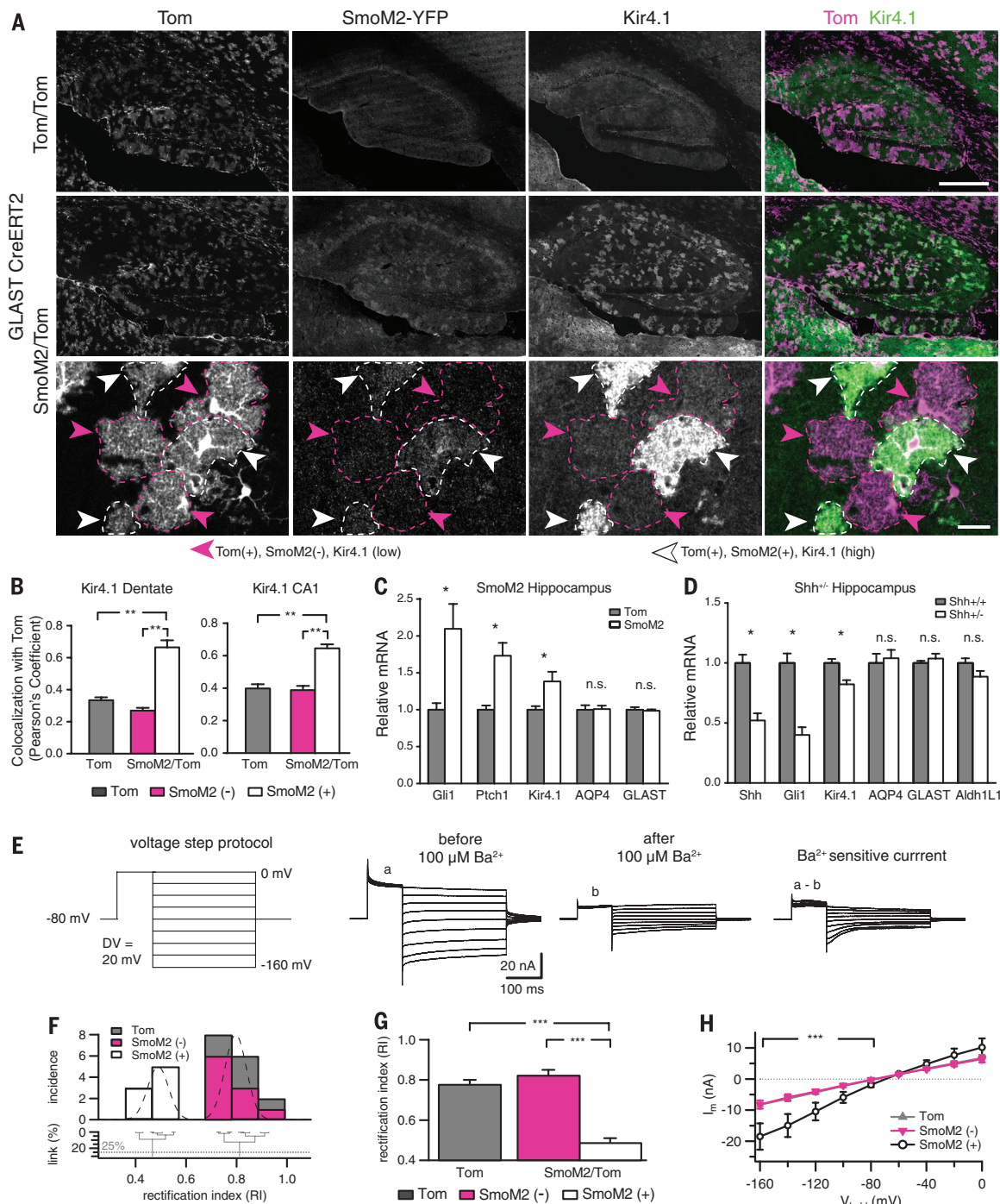


Fig. 4. Shh signaling controls hippocampal astrocytes.

(A) Astrocytes containing SmoM2 (white arrowheads) or not (magenta arrowheads). Cre was activated at 5 weeks with mice analyzed 4 weeks later. **(B)** Quantification of Kir4.1 expression in CA1 and dentate gyrus through fluorescence colocalization with Tomato reference protein ($n = 4$ pairs). One-way ANOVA with Tukey's. **(C)** mRNA levels in hippocampus (>5 weeks; 2 weeks after Cre induction; $n = 7$ control and 8 SmoM2 mice). Student's t test. **(D)** mRNA levels in Shh haploinsufficient mice (>5 weeks; $n = 6$ pairs). Student's t test. **(E to H)** Ba²⁺-sensitive Kir4.1 currents in astrocytes 2 weeks after SmoM2 expression. **(E)** (Left) Voltages were stepped from -160 to 0 mV, with initial step to inactivate non-Kir K⁺ currents. (Middle, right) Representative currents before (a) and after (b) Ba²⁺, with Kir4.1 current determined by subtraction (a – b). **(F and G)** Hierarchical clustering analysis-grouped SmoM2(-) ($n = 6$ cells) with controls (Tom, $n = 10$) but segregated SmoM2(+), ($n = 8$).

(H) SmoM2(+) Ba²⁺-sensitive current-voltage curve differed below the reversal potential. Wilcoxon-Mann-Whitney test. Error bars represent SEM. * $P \leq 0.05$, ** $P \leq 0.01$, *** $P \leq 0.001$. **(A)** Scale bars, $500 \mu\text{m}$ and $20 \mu\text{m}$.

in the mature brain (6, 7). These factors likely cooperate with developmental patterning events to generate astrocyte heterogeneity (10, 11, 29) and ultimately ensure that astrocytes are properly specialized for the needs of local neural circuits (30).

REFERENCES AND NOTES

- V. Matyash, H. Kettenmann, *Brain Res. Brain Res. Rev.* **63**, 2–10 (2010).
- Y. Zhang, B. A. Barres, *Curr. Opin. Neurobiol.* **20**, 588–594 (2010).
- N. A. Oberheim, S. A. Goldman, M. Nedergaard, *Methods Mol. Biol.* **814**, 23–45 (2012).
- A. V. Gourine et al., *Science* **329**, 571–575 (2010).
- A. S. Saab et al., *Science* **337**, 749–753 (2012).
- J. D. Cahoy et al., *J. Neurosci.* **28**, 264–278 (2008).
- Y. Zhang et al., *J. Neurosci.* **34**, 11929–11947 (2014).
- M. R. Freeman, *Science* **330**, 774–778 (2010).
- Y. Muroyama, Y. Fujiwara, S. H. Orkin, D. H. Rowitch, *Nature* **438**, 360–363 (2005).
- C. Hochstim, B. Deneen, A. Lukaszewicz, Q. Zhou, D. J. Anderson, *Cell* **133**, 510–522 (2008).
- H. H. Tsai et al., *Science* **337**, 358–362 (2012).
- M. R. Freeman, D. H. Rowitch, *Neuron* **80**, 613–623 (2013).
- K. Yamada, M. Watanabe, *Anat. Sci. Int.* **77**, 94–108 (2002).
- Y. Kita, K. Kawakami, Y. Takahashi, F. Murakami, *PLOS ONE* **8**, e70091 (2013).
- T. M. Hoogland, B. Kuhn, *Cerebellum* **9**, 264–271 (2010).
- M. C. Papadopoulos, A. S. Verkman, *Nat. Rev. Neurosci.* **14**, 265–277 (2013).

17. M. Fuccillo, A. L. Joyner, G. Fishell, *Nat. Rev. Neurosci.* **7**, 772–783 (2006).
18. J. Briscoe, *EMBO J.* **28**, 457–465 (2009).
19. T. Mori et al., *Glia* **54**, 21–34 (2006).
20. F. Long, X. M. Zhang, S. Karp, Y. Yang, A. P. McMahon, *Development* **128**, 5099–5108 (2001).
21. B. Djukic, K. B. Casper, B. D. Philpot, L.-S. Chin, K. D. McCarthy, *J. Neurosci.* **27**, 11354–11365 (2007).
22. R. V. Pearse 2nd, K. J. Vogan, C. J. Tabin, *Dev. Biol.* **239**, 15–29 (2001).
23. J. Jeong, J. Mao, T. Tenzen, A. H. Kottmann, A. P. McMahon, *Genes Dev.* **18**, 937–951 (2004).
24. A. D. R. Garcia, R. Petrova, L. Eng, A. L. Joyner, *J. Neurosci.* **30**, 13597–13608 (2010).
25. C. C. Harwell et al., *Neuron* **73**, 1116–1126 (2012).
26. L. E. Gonzalez-Reyes et al., *Neuron* **75**, 306–319 (2012).
27. M. K. Cooper, J. A. Porter, K. E. Young, P. A. Beachy, *Science* **280**, 1603–1607 (1998).
28. A. Rohner et al., *Mol. Cancer Ther.* **11**, 57–65 (2012).

29. A. V. Molofsky et al., *Nature* **509**, 189–194 (2014).
30. X. Tong et al., *Nat. Neurosci.* **17**, 694–703 (2014).

ACKNOWLEDGMENTS

Glast-CreERT2 mice are available from M. Götz under a material transfer agreement with Helmholtz Zentrum München–Deutsches Forschungszentrum für Gesundheit und Umwelt. This work was supported by the Canadian Institutes of Health Research (FDN 143337 to C.W.B., MOP 126137/NIA 288936 to P.J.S., and MOP 111152/MOP 123390 to K.K.M.); Natural Sciences and Engineering Research Council of Canada (DG 418546-2 to P.J.S. and 408044-2011 to K.K.M.); Canada Research Chairs Program (F.C., C.E., and K.K.M.); Brain Canada/W. Garfield Weston Foundation (F.C. and K.K.M.); James McGill Chair Program (C.W.B.); and Canadian Foundation for Innovation (LOF 28331 to P.J.S.). W.T.F. was supported by a postdoctoral fellowship from the Research Institute of the McGill University Health Centre. J.P. was supported by a

Vanier fellowship. We thank M. Götz for GLAST CreERT2 mice; G. Quesseveur for help with tissue processing; L. Li for mouse technical assistance; S. Scales (Genentech) for Shh antibody; T. Alves-Ferreira for ImageJ support; A. Montpetit, A. Staffa, and staff at Genome Quebec and the Research Institute of McGill University Hospital Centre Molecular Imaging Platform for support and use of instrumentation; and E. Ruthazer and D. van Meyel for helpful feedback on the manuscript. The authors declare no conflicts of interest.

SUPPLEMENTARY MATERIALS

www.sciencemag.org/content/351/6275/849/suppl/DC1
Materials and Methods
Figs. S1 to S25
Tables S1 to S5
References (31–40)

21 April 2015; accepted 7 January 2016
10.1126/science.aab3103

MICROBIOME

Lactobacillus plantarum strain maintains growth of infant mice during chronic undernutrition

Martin Schwarzer,^{1,2*} Kassem Makki,^{1,3} Gilles Storelli,¹ Irma Machuca-Gayet,^{1†} Dagmar Srutkova,² Petra Hermanova,² Maria Elena Martino,¹ Severine Balmand,⁴ Tomas Hudcovic,² Abdelaziz Heddi,⁴ Jennifer Rieusset,³ Hana Kozakova,² Hubert Vidal,³ François Leulier^{1*}

In most animal species, juvenile growth is marked by an exponential gain in body weight and size. Here we show that the microbiota of infant mice sustains both weight gain and longitudinal growth when mice are fed a standard laboratory mouse diet or a nutritionally depleted diet. We found that the intestinal microbiota interacts with the somatotrophic hormone axis to drive systemic growth. Using monocolonized mouse models, we showed that selected lactobacilli promoted juvenile growth in a strain-dependent manner that recapitulated the microbiota's effect on growth and the somatotrophic axis. These findings show that the host's microbiota supports juvenile growth. Moreover, we discovered that lactobacilli strains buffered the adverse effects of chronic undernutrition on the postnatal growth of germ-free mice.

During the juvenile growth period, the gain in animal body size varies widely as a result of the interactions between nutritional input and the organism's hormonal cues. In mammals, postnatal growth is controlled by the activity of the somatotrophic axis (fig. S1), in

which growth hormone (GH) instructs the liver and peripheral tissues to produce insulin-like growth factor-1 (IGF-1), to promote organ and systemic growth (1–3). Chronic undernutrition triggers a state of GH resistance (4, 5) that leads to stunting, and juveniles become small and thin (6). Acute malnutrition, in contrast, causes wasting, defined as severe weight loss and mediated in part through the disruption of the gut microbiota (7). However, the contribution of the gut microbiota to normal postnatal growth and its influence on the activity of the somatotrophic axis during chronic undernutrition remain unknown.

To address this question, we first compared the growth parameters of wild-type (WT) and germ-free (GF) infant male mice fed a standard breeding diet (25% proteins, 9% fats; table S1) until young adulthood (8 weeks old, Fig. 1 and fig. S2). After weaning, the GF and WT animals ingested similar amounts of food relative to body weight (fig. S3), yet at 8 weeks of age, GF mice weighed 14.5% less and were 4% shorter than

WT mice (Fig. 1, A and C; fig. S2, A and B; and table S2). These growth differences were most pronounced after weaning (Fig. 1, A to D, and fig. S2, C and D). Thus, with a standard breeding diet, the gut microbiota ensures optimal weight gain and longitudinal growth, especially around weaning. Remarkably, the 17% weight gain seen in WT animals (fig. S2A and table S2) was not a consequence of increased adiposity. The epididymal fat pads and adipocyte size of WT and GF males remained similar (fig. S4, A to D). Likewise, levels of leptin, a circulating marker of fat stores (8), were similar in the sera of WT and GF animals (fig. S4E). However, the weight gain of the organs of WT animals was greater than that of GF mice (fig. S2E and table S2), confirming that a WT microbiota is associated with optimal systemic somatic growth. This contrasts with the increased adiposity that results from subtherapeutic antibiotic treatments in infant mice that is apparently caused by disrupting the gut microbiota community (9, 10). WT animals were 4% longer (fig. S2B and table S2), indicating that the microbiota also influences skeletal growth. Bone growth parameters, including femur length, cortical thickness, cortical bone fraction, and the trabecular fraction of the femur (Fig. 1, E and F; fig. S2, F to I; and table S2) were all reduced in GF animals, although cortical bone mineral density (BMD) was unaffected (fig. S2J). Previously, Sjögren et al. showed that trabecular BMD was increased in GF animals relative to their WT siblings (11). However, that study was conducted on females of a different genetic background than ours. Nevertheless, taken together, our results show that the gut microbiota sustains postnatal somatic tissue growth, leading to increased mass gain and enhanced longitudinal growth.

Postnatal systemic growth is mainly driven by the activity of the somatotrophic axis (1–3), where the pituitary gland produces GH, which induces the production of IGF-1. The liver is the major source of circulating IGF-1 and together with IGF-1 binding protein-3 (IGFBP-3) serves as an endocrine determinant of somatic growth (3, 12, 13) (fig. S1). In addition, IGF-1 is produced by peripheral tissues, including muscles, and acts to promote tissue growth in an autocrine/paracrine manner

¹Institut de Génétique Fonctionnelle de Lyon, Université de Lyon, Ecole Normale Supérieure de Lyon, Centre National de la Recherche Scientifique, Université Claude Bernard Lyon 1, Unité Mixte de Recherche 5242, 46 Allée d'Italie, 69364 Lyon Cedex 07, France. ²Laboratory of Gnotobiology, Institute of Microbiology of the Czech Academy of Sciences, v. v. i., Novy Hradek, Czech Republic. ³Laboratoire CarMeN, Université Lyon 1, Unité Mixte de Recherche INSERM U-1060 et INRA U-1397, Faculté de Médecine Lyon-Sud, Chermieu du Grand Revoyet, 69600 Oullins, France. ⁴UMR203 BF21, Biologie Fonctionnelle Insectes et Interactions, Université de Lyon, INRA, INSA-Lyon, F-69621 Villeurbanne, France.

*Corresponding author. E-mail: francois.leulier@ens-lyon.fr (F.L.); martin.schwarzer@ens-lyon.fr (M.S.) †Present address: Institut National de la Santé et de la Recherche Médicale, Université Claude Bernard Lyon 1, Unité Mixte de Recherche 1033, Faculté de Médecine Lyon-Est, Rue Guillaume Paradin, 69372 Lyon Cedex 08, France.



Neurons diversify astrocytes in the adult brain through sonic hedgehog signaling

W. Todd Farmer *et al.*
Science **351**, 849 (2016);
DOI: 10.1126/science.aab3103

This copy is for your personal, non-commercial use only.

If you wish to distribute this article to others, you can order high-quality copies for your colleagues, clients, or customers by [clicking here](#).

Permission to republish or repurpose articles or portions of articles can be obtained by following the guidelines [here](#).

The following resources related to this article are available online at www.sciencemag.org (this information is current as of March 17, 2016):

Updated information and services, including high-resolution figures, can be found in the online version of this article at:

</content/351/6275/849.full.html>

Supporting Online Material can be found at:

</content/suppl/2016/02/17/351.6275.849.DC1.html>

A list of selected additional articles on the Science Web sites **related to this article** can be found at:

</content/351/6275/849.full.html#related>

This article **cites 40 articles**, 15 of which can be accessed free:

</content/351/6275/849.full.html#ref-list-1>

This article has been **cited by** 1 articles hosted by HighWire Press; see:

</content/351/6275/849.full.html#related-urls>

This article appears in the following **subject collections**:

Neuroscience

</cgi/collection/neuroscience>